11362 *Inorg. Chem.* **2009**, *48*, 11362–11375
DOI: 10.1021/ic901914n

Inorganic Chemistry
Article

Luminescent Copper(I) Halide Butterfly Dimers Coordinated to $[Au(CH_3imCH_2py)_2]BF_4$ and $[Au(CH_3imCH_2quin)_2]BF_4$

Vincent J. Catalano,*,† Adam L. Moore,† Jason Shearer,† and Jineun Kim‡

†*Department of Chemistry, University of Nevada, Reno, Nevada 89557 and* ‡*Department of Chemistry (BK21) and Research Institute of Natural Science, Gyeongsang National University, Jinju 660-701, South Korea*

Received September 28, 2009

The coordination chemistry of copper(I) halides to the homoleptic, N-heterocyclic carbene Au(I) complexes $[Au(CH_3imCH_2quin)_2]BF_4$ and $Au(CH_3imCH_2py)_2]BF_4$ was explored. The reaction of CuX (X = Cl, Br, I) with either $[Au(CH_3imCH_2quin)_2]BF_4$ or $[Au(CH_3imCH_2py)_2]BF_4$ produces trimetallic complexes containing Cu_2X_2-butterfly copper clusters coordinated to the two imine moieties. The triangular arrangement of the metals places the gold(I) center in close proximity (~2.5−2.6 Å) to the centroid of the Cu−Cu vector. The Cu−Cu separations vary as a function of bridging halide with the shortest Cu−Cu separations of ~2.5 Å found in the iodo-complexes and the longest separations of 2.9 Å found in the bridging chloride complexes. In all six complexes the Au−Cu separations range from ~2.8 to 3.0 Å. In the absence of halides, the dimetallic complex $[AuCu(CH_3imCH_2py)_2(NCCH_3)_2](BF_4)_2$, containing a long Au−Cu distance of ~4.72 Å is formed. Additionally, as the byproduct of the reaction of CuBr with $[Au(CH_3imCH_2quin)_2]BF_4$ the deep-red, dimetallic compound, $AuCuBr_2(CH_3imCH_2quin)_2$, was isolated in very low yield. All of these complexes were studied by NMR spectroscopy, mass spectrometry, and the copper containing species were additionally characterized by X-ray crystallography. In solution the copper centers dissociate from the gold complexes, but as shown by XANES and EXAFS spectroscopy, at low temperature the Cu−Cu linkage is broken, and the individual copper(I) halides reposition themselves to opposite sides of the gold complex while remaining coordinated to one imine moiety. In the solid state all of the complexes are photoluminescent, though the nature of the excited state was not determined.

Introduction

Attractive interactions between d^{10} closed shell metal ions have garnered considerable attention because of their unusual bonding and interesting optical properties.[1−4] Of the closed shell attractions, Au(I)−Au(I) interactions are the most studied,[5,6] and the nature of this *aurophilic*[7] attraction is largely attributed to dispersion.[8] Additionally, incorporation of a dissimilar metal, such as Cu(I), into the coordination environment greatly alters the electronic and photophysical properties.[9,10] For example, the tetranuclear complex $[\{AuCu(\mu\text{-Spy})(\mu\text{-PPh}_2\text{py})\}_2](PF_6)_2$ reported by Eisenberg and co-workers[11] shows an intense emission band at 610 nm which is red-shifted relative to its monometallic Au(I) starting material. Further, Fernández et al.[12] reported the highly luminescent, Au(I)−Cu(I) coordination polymer, $[Cu\{Au(C_6F_5)_2(NCCH_3)(\mu_2\text{-}C_4H_4N_2)\}]_n$, containing Au(I)−Cu(I) distances of 2.8216(6) Å. This complex forms a one-dimensional polymeric chain through unsupported Au(I)···Cu(I) interactions. More recently they have extended this work to explore the influence of ancillary ligand coordination and reported several discrete gold−copper complexes with unsupported metal−metal interactions.[13]

*To whom correspondence should be addressed. E-mail: vjc@unr.edu.

(1) Pyykkö, P. *Chem. Rev.* **1997**, *97*, 597.
(2) Forward, J. M.; Fackler, J. P., Jr.; Assefa, Z. In *Optoelectronic Properties of Inorganic Compounds*; Roundhill, D. M., Fackler, J. P., Jr., Eds.; Plenum: New York, 1999; pp 195−226.
(3) Katz, M. J.; Sakai, K.; Leznoff, D. B. *Chem. Soc. Rev.* **2008**, *37*, 1884.
(4) Yam, V. W.-W.; Cheng, W. W.-C. *Chem. Soc. Rev.* **2008**, *37*, 1806.
(5) Schmidbaur, H.; Schier, A. *Chem. Soc. Rev.* **2008**, *37*, 1931.
(6) Schmidbaur, H. *Gold Bull.* **2000**, *33*, 3.
(7) Schmidbaur, H.; Cronje, S.; Djordjevic, B.; Schuter, O. *Chem. Phys.* **2005**, *311*, 151.
(8) Pyykkö, P. *Chem. Soc. Rev.* **2008**, *37*, 1967.
(9) Fernández, E. J.; Laguna, A.; López-de-Luzuriaga, J. M. *Dalton Trans.* **2007**, 1969.
(10) Fernández, E. J.; Laguna, A.; López-de-Luzuriaga, J. M.; Monge, M.; Montiel, M.; Olmos, M. E.; Rodríguez-Castillo, M. *Organometallics* **2006**, *25*, 3639.
(11) Hao, L.; Mansour, M. A.; Lachicotte, R. J.; Gysling, H. J.; Eisenberg, R. *Inorg. Chem.* **2000**, *39*, 5520.
(12) Fernández, E. J.; Laguna, A.; López-de-Luzuriaga, J. M.; Monge, M.; Montiel, M.; Olmos, M. E. *Inorg. Chem.* **2005**, *44*, 1163.
(13) Fernández, E. J.; Laguna, A.; López-de-Luzuriaga, J. M.; Monge, M.; Montiel, M.; Olmos, M. E.; Rodríguez-Castillo, M. *Dalton Trans.* **2009**, 7509.

Published on Web 11/09/2009

Metallophilic attractions involving copper(I) are less well-represented in the literature,[14−20] yet many Cu(I) complexes with considerable metal−metal interactions are known to exhibit photoluminescence.[21] Of these, copper(I) halide complexes coordinated to substituted pyridyl substituents are some of the most well-studied.[22−24] For example, Araki et al. reported the preparation and optical properties of the dimetallic $[Cu_2(\mu\text{-}X)_2(PPh_3)_2(L)_n]$ (X = I, Br; L = 4,4′-bipyridine, pyrazine, pyrimidine, 1,5-naphthyridine, 1,6-naphthyridine, quinazoline, *N*,*N*-dimethyl-4-aminopyridine, 3-benzoylpyridine, 4-benzoylpyridine, piperazine; n = 1, 2) complexes and demonstrated that the emission can be easily tuned by altering the coordinating N-heteroaromatic ligand.[25] With the emission energies roughly correlating to the reduction potential of the imine ligands, the authors assigned the excited state to a Metal-to-Ligand Charge-Transfer (MLCT) state.

Moreover, multimetallic copper(I) halide complexes can adopt a number of structural motifs including cubic tetranuclear cores ($(LCuX)_4$), infinite polymeric staircases ($(LCuX)_n$), and discrete dimetallic species ($(LCuX)_2$).[26] The cubic, four-coordinate tetranuclear core is quite common and has been known for some time.[27−29] In this motif, four Cu(I) centers reside on opposing corners of a cube while triply bridging halide atoms occupy the remaining corners. Each Cu(I) is additionally coordinated to an ancillary ligand, often a phosphine or imine. In the staircase structure, the monometallic unit is composed of a copper(I) center that is linearly bound to both the halide and ancillary moiety. The infinite chains are formed by the stacking of monometallic units in an opposing manner so that the Cu−X portion of two individual units form a rhomboid.[30,31]

Recently, we reported the coordination chemistry of pyridyl-substituted NHC ligands and their corresponding Au(I) and Ag(I) complexes.[32−37] The pyridyl moieties of the NHC ligands are ideally suited to coordinate to a dissimilar metal and orient it in close proximity to the gold center. Given the interesting coordination and optical properties of Cu(I) and its halide clusters we questioned whether copper halide clusters could be assembled near the Au(I) center. Here, we explore the addition of Cu(I) to the Au(I) containing NHC complexes $[Au(CH_3imCH_2py)_2]^+$ and $[Au(CH_3imCH_2quin)_2]^+$.

Experimental Section

Solvents were used as received without purification or drying. The preparations of $[Au(CH_3imCH_2py)]BF_4$[32] and Au(tht)Cl[38] (tht is tetrahydrothiophene) were described elsewhere. UV−vis spectra were obtained using a Hewlett-Packard 8453 diode array spectrometer (1 cm path-length cells). Emission data were recorded using a Spex Flouromax steady-state fluorimeter. Mass spectra data were collected using a Waters Mass Spectrometer, and Columbia Analytics performed the elemental analysis.

X-ray Crystallography. For all complexes X-ray quality crystals were obtained by slow diffusion of diethyl ether into acetonitrile or benzonitrile solution of the complexes. Suitable crystals were coated in hydrocarbon oil and mounted on a glass fiber. X-ray crystallographic data were collected at low temperature (100 K) using Bruker SMART Apex CCD diffractometer with Mo K_α radiation and a detector-to-crystal distance of 4.94 cm. Data were collected with 0.5° scans in ω and φ using exposure times of 10−60 s per frame. Typically, the 2θ range extended from 3.0 to 55°. Data were corrected for Lorentz and polarization effects using the SAINT program and corrected for absorption using SADABS or TWINABS. Unit cells were indexed and refined using up to 9999 reflections harvested from the data collection. The structures were solved by direct methods and refined using the SHELXTL 6.10 software package.[39] Crystallographic parameters are listed in Tables 1 and 2.

Cu K-Edge X-ray Absorption Sample Preparation and Data Collection. Solid state samples of $[AuCu_2X_2(CH_3imCH_2py)_2]BF_4$ and $[AuCu_2X_2(CH_3imCH_2quin)_2]BF_4$ (X = Cl or Br) were prepared by finely grinding powders of the metal compounds in Nujol (final concentrations ∼9 mM) and placing the resulting pastes in aluminum sample holders, and sealing the paste between windows made from Kapton tape. Acetonitrile solution samples were made by dissolving the metal complexes in CH_3CN (final concentrations ∼2 mM), injecting the solutions in aluminum sample holders between windows made from Kapton tape, and quickly freezing the solutions in liquid nitrogen. Data were collected at the National Synchrotron Light Source (Upton, NY) on beamline X3b. All samples were maintained at 20 K throughout data collection using a helium Displex cryostat. Data were collected in fluorescence mode using a 13 element Ge solid state collector (Canberra), which was covered with a 6 μm Ni filter for background rejection . Total count rates were maintained under 20 kHz per channel, and a deadtime correction was not employed. X-ray beam energies were selected using a focused Si(111) double monochromator, and a low-angle (4.5 mrad) polished Ni mirror was used for higher order harmonic rejection. Energy calibrations were accomplished by simultaneously recording the X-ray absorption spectrum of Cu foil (first inflection point set to 8980.3 eV). All spectra represent the averaged sum of 3 individual spectra for the chloride containing compounds and 6 individual spectra for the bromide containing compounds.

(14) Carvajal, M. A.; Alvarez, S.; Novoa, J. J. *Chem.—Eur. J.* **2004**, *10*, 2117.
(15) Sugiura, T.; Yoshikawa, H.; Awaga, K. *Inorg. Chem.* **2006**, *45*, 7584.
(16) Zhang, X. M.; Hao, Z.-M.; Wu, H.-S. *Inorg. Chem.* **2005**, *44*, 7301.
(17) Zhang, J.-P.; Wang, Y.-B.; Huang, X.-C.; Lin, Y.-Y.; Chen, X.-M. *Chem.—Eur. J.* **2005**, *11*, 552.
(18) Che, C.-M.; Mao, Z.; Miskowski, V. M.; Tse, M.-C.; Chan, C.-K.; Cheung, K.-K.; Phillips, D. L.; Leung, K.-H. *Angew. Chem., Int. Ed.* **2000**, *39*, 4084.
(19) Poblet, J.-M.; Bénard, M. *Chem. Commun.* **1998**, 1179.
(20) Siemeling, U.; Vorfeld, U.; Neumann, B.; Stammler, H.-G. *Chem. Commun.* **1997**, 1723.
(21) Ford, P. C.; Cariati, E.; Bourassa, J. *Chem. Rev.* **1999**, 3625.
(22) Vitale, M.; Ford, P. C. *Coord. Chem. Rev.* **2001**, *219−221*, 3.
(23) Ryu, C. K.; Vitale, M.; Ford, P. C. *Inorg. Chem.* **1993**, *32*, 869.
(24) Kyle, K. R.; Ryu, C. K.; DiBenedetto, J. A.; Ford, P. C. *J. Am. Chem. Soc.* **1991**, *113*, 2954.
(25) Araki, H.; Tsuge, K.; Sasaki, Y.; Ishizaka, S.; Kitamura, N. *Inorg. Chem.* **2005**, *44*, 9667.
(26) Graham, P. M.; Pike, R. D.; Sabat, M.; Bailey, R. D.; Pennington, W. T. *Inorg. Chem.* **2000**, *39*, 5121.
(27) Raston, C. L.; White, A. H. *J. Chem. Soc., Dalton Trans.* **1976**, 2153.
(28) Rath, N. P.; Maxwell, J. L.; Holt, E. M. *J. Chem. Soc., Dalton Trans.* **1986**, 2449.
(29) Dyason, J. C.; Healy, P. C.; Pakawatchai, C.; Patrick, V. A.; White, A. H. *Inorg. Chem.* **1985**, *24*, 1957.
(30) Lee, S.; Park, S.; Kang, Y.; Moon, S.-H.; Lee, S. S.; Park, K.-M. *Bull. Korean Chem. Soc.* **2008**, *29*, 1811.
(31) Bosch, E.; Barnes, C. L. *J. Coord. Chem. Rev.* **2003**, *53*, 329.
(32) Catalano, V. J.; Moore, A. L. *Inorg. Chem.* **2004**, *44*, 6558.
(33) Catalano, V. J.; Etogo, A. O. *Inorg. Chem.* **2007**, 5608.
(34) Ghosh, A. K.; Catalano, V. J. *Eur. J. Inorg. Chem.* **2009**, 1832.
(35) Catalano, V. J.; Etogo, A. O. *J. Organomet. Chem.* **2005**, *690*, 6041.
(36) Catalano, V. J.; Malwitz, M. A.; Etogo, A. O. *Inorg. Chem.* **2004**, *43*, 5714.
(37) Catalano, V. J.; Malwitz, M. A. *Inorg. Chem.* **2003**, *42*, 5483.
(38) Uson, R.; Laguna, A.; Laguna, M. *Inorg. Synth.* **1989**, *26*, 85.
(39) Sheldrick, G. M. *SHELXTL: Structure Determination Software Suite*, Version 6.10; Bruker AXS: Madison WI, 2001.

Table 1. Crystallographic Data for **4**−**7**

	4	**5**·PhCN	**6**·CH_3CN	**7**
formula	$C_{28}H_{26}N_6AuCu_2Cl_2BF_4$	$C_{35}H_{31}N_7AuCu_2Br_2BF_4$	$C_{30}H_{26}N_7AuCu_2I_2BF_4$	$C_{28}H_{26}N_6AuCuBr_2$
fw	928.30	1120.34	1149.23	866.87
crystal system	monoclinic	triclinic	monoclinic	monoclinic
space group	$P2(1)/c$	$P\bar{1}$	$P2(1)/n$	$P2(1)/c$
a, Å	9.8762(11)	10.4526(7)	10.513(3)	10.8582(1)
b, Å	32.362(5	11.8432(9)	25.914(7)	8.8845(1)
c, Å	9.4702(12)	15.7913(11)	13.379(4)	28.0213(4)
α, deg	90	102.612(5)	90	90
β, deg	103.339(7)	102.575(5)	109.974(16)	94.056(1)
γ, deg	90	101.806(5)	90	90
V, Å	2945.2(6)	1795.5(2)	3425.6(16)	2696.44(5)
Z	4	2	4	4
temp, K	100(2)	100(2)	100(2)	100(2)
R_1	0.0645	0.0605	0.0935	0.0347
wR_2 ($I > 2\sigma(I)$)	0.1370	0.1468	0.1626	0.0889

Table 2. Crystallographic Data for Complexes **9**−**12**

	9	**10**	**11**·0.5H_2O·0.25 Et_2O	**12**·0.25CH_3CN
formula	$C_{20}H_{22}N_6AuCu_2Cl_2BF_4$	$C_{20}H_{22}N_6AuCu_2Br_2BF_4$	$C_{20}H_{22}N_6AuCu_2I_2BF_4O$	$C_{26}H_{22}N_9AuCuB_2F_8$
fw	828.19	917.11	1027.09	894.65
crystal system	triclinic	triclinic	monoclinic	monoclinic
space group	$P\bar{1}$	$P\bar{1}$	$C2/c$	$P2(1)/c$
a, Å	9.9580(5)	9.9074(2)	10.5411(3)	15.3313(4)
b, Å	10.3384(5)	10.2809(2)	31.7301(11)	21.5103(6)
c, Å	12.7149(6)	13.1628(2)	19.8835(6)	10.3570(3)
α, deg	98.906(3)	98.4330(10)	90	90
β, deg	100.388(3)	102.0750(10)	96.305(2)	106.027(2)
γ, deg	99.722(2)	97.5990(10)	90	90
V, Å	1245.66(10)	1278.36(4)	6610.2(4)	3282.78(16)
Z	2	2	8	4
temp, K	100(2)	100(2)	100(2)	100(2)
R_1	0.0334	0.0304	0.0636	0.0451
wR_2 ($I > 2\sigma(I)$)	0.0650	0.0531	0.1433	0.0800

Cu K-Edge X-ray Absorption Data Analysis. Prior to data averaging, each spectrum was individually inspected to determine if photodecomposition was occurring between scans, and each detector channel was individually inspected. All spectra that showed signs of photodecomposition were rejected prior to data averaging. Data workup and analysis was performed as previously described using EXAFS123, which consists of a series of macros and procedures written for the software package Igor Pro version 6.02 (Wavemetrics; Lake Oswego, OR). Peak positions in the XANES spectra were obtained by examining the second derivative of the XANES spectra. Phase and amplitude functions for all single scattering Cu−N, Cu−Au, Cu-halide, and Cu−C were made as previously described from simulations of the EXAFS spectra of $[AuCu_2X_2(CH_3imCH_2py)_2]BF_4$ and $[AuCu_2X_2(CH_3imCH_2quin)_2]BF_4$ created from their crystal structures and the software package FEFF 8.4. The data were refined as previously described, except the number of scatterers per shell were restrained to the nearest whole number following an initial refinement as a free parameter. Fits to the spectra were judged using the goodness of fit parameter:

$$\mathrm{GOF} = \mathrm{average}[(\chi - \chi_{\mathrm{sim}})/\mathrm{esd}_{\mathrm{data}}](n_i/(n_i - n_p))^{1/2}$$

where n_i is the number of independent data points and n_p is the number of parameters in the data simulation. All EXAFS analysis performed herein were performed on unfiltered $k^3(\chi)$ data over the range of k = 2.0−14.5 Å^{-1} for $[AuCu_2Br_2(CH_3imCH_2py)_2]BF_4$ and $[AuCu_2Br_2(CH_3imCH_2quin)_2]BF_4$ or 2.0−12.0 Å^{-1} for $[AuCu_2Cl_2(CH_3imCH_2py)_2]BF_4$ and $[AuCu_2Cl_2(CH_3imCH_2quin)_2]BF_4$.

[H(CH$_3$imCH$_2$quin)]BF$_4$, 1. A 50 mL round-bottom flask was charged with 0.500 g (2.33 mmol) of quinolylchloride hydrochloride, 0.403 g (2.92 mmol) of K_2CO_3, and 25 mL of acetone. The mixture was refluxed for 30 min. After which 0.191 g (2.33 mmol) of 1-methylimidazole was added, followed by 0.280 g (2.56 mmol) of $NaBF_4$, and the mixture was further refluxed for 3 days. After cooling, the mixture was filtered through Celite. The filtrate was evaporated to dryness, and 15 mL of CH_2Cl_2 was added. The insoluble salts were removed by filtration, and the filtrate concentrated to about 5 mL. Complex **1** was precipitated as a white solid (0.262 g, (0.842 mmol, 36%)) by slow addition of diethyl ether. ^{1}H NMR (400 MHz, CD_3CN) δ 9.28 (s, 1H), 8.35 (d, J = 8.4, 1H), 7.95 (d, J = 8.4, 2H), 7.77 (t, J = 7.7, 1H), 7.69−7.52 (m, 3H), 7.42 (s, 1H), 5.74 (s, 2H), 3.91 (s, 3H). ^{13}C NMR (126 MHz, CD_3CN) δ 155.23, 148.83, 139.08, 138.98, 131.57, 130.20, 129.33, 128.98, 128.50, 124.69, 124.62, 121.42, 55.27, 37.36. UV−vis (CH_3CN) λ_{max}, nm (ε): 274 (3490), 316 (2950), 302 (2930). Mass ESI MS: M^+ = 224.2. Anal. Calcd ($C_{14}H_{14}N_4BF_4$) (%). C, 54.05; H, 4.54; N, 13.51. Found: C, 53.72; H, 4.52; N, 13.68.

[Ag(CH$_3$imCH$_2$quin)$_2$]BF$_4$, 2. A 50 mL round-bottom flask was charged with 0.050 g (0.161 mmol) of $[H(CH_3imCH_2quin)]BF_4$, 25 mL of CH_2Cl_2, 0.016 g (0.008 mmol) of $AgBF_4$, and about 5 mg of Bu_4NBF_4. The mixture was protected from light and stirred for 10 min at room temperature. NaOH (1 N, 3 mL) was then added, and stirring was continued for 30 min. The mixture was filtered through Celite, and the clear filtrate was reduced to minimum volume under vacuum. Complex **2** was precipitated as a white powder (0.060 g (0.094 mmol, 87%)) by slow addition of diethyl ether. ^{1}H NMR (400 MHz, CD_3CN) δ 8.12 (d, J = 8.4, 2H), 7.85−7.78 (m, 3H), 7.77 (s, 1H), 7.65 (dd, J = 6.2, 7.7, 2H), 7.53 (t, J = 7.7, 1H), 7.32 (d, J = 1.8, 2H), 7.22 (d, J = 8.4, 2H), 7.17 (d, J = 1.8, 2H), 5.47 (s, 6H), 3.72 (s, 9H), ^{13}C NMR (126 MHz, CD_3CN) δ 183.15, 157.50, 148.40, 138.44,

Scheme 1

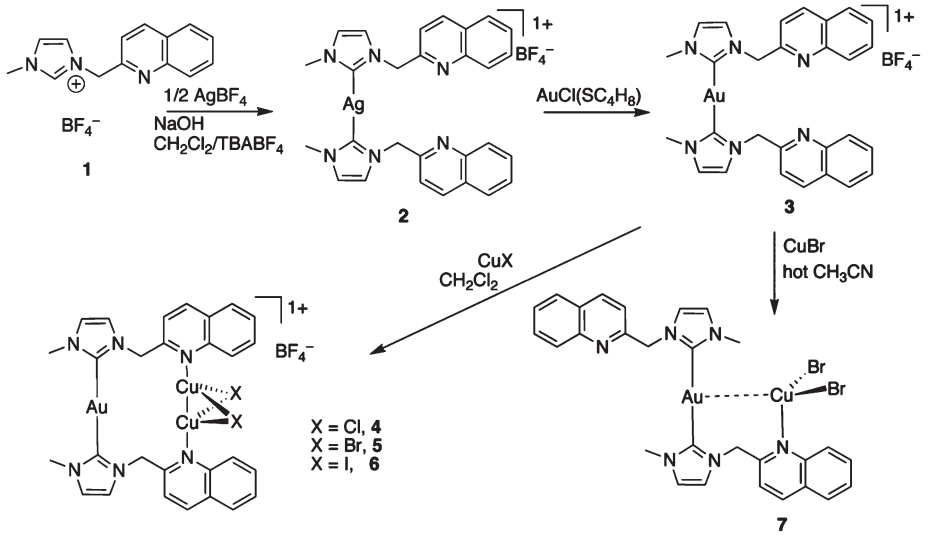

131.05, 129.63, 128.90, 128.40, 128.06, 127.88, 123.70, 123.69, 120.75, 57.85, 39.21. λ_{max}, nm (ε): 274 (9690), 316 (6980), 303 (7240). Mass ESI MS: M^+ = 554. Anal. Calcd ($C_{28}H_{26}N_6AgBF_4$) (%). C, 52.45; H, 4.09; N, 13.11. Found: C, 52.37; H, 4.33; N, 12.89.

[Au(CH$_3$imCH$_2$quin)$_2$]BF$_4$, 3. A 25 mL round-bottom flask was charged with 0.055 g (0.086 mmol) of **2**, and 10 mL of CH_2Cl_2. Au(tht)Cl (0.027 g, (0.086 mmol)) in 5 mL of CH_2Cl_2 was added dropwise. The mixture was protected from light and stirred for 15 min during which time a precipitate formed. The solution was filtered through Celite removing the precipitated AgCl. The clear filtrate was subsequently reduced to 5 mL, and a white powder was precipitated with diethyl ether (0.054 g (0.074 mmol, 86%)). ^{1}H NMR (400 MHz, CD_3CN) δ 8.08 (d, J = 8.4, 1H), 7.80 (dd, J = 8.4, 13.6, 2H), 7.6 (t, J = 7.0, 1H), 7.51 (t, J = 7.6, 1H), 7.31 (d, J = 1.8, 1H), 7.20 (d, J = 1.8, 2H), 7.17 (s, 1H), 5.51 (s, 2H), 3.74 (s, 3H). ^{13}C NMR (101 MHz, CD_3CN) δ 185.93, 157.16, 148.36, 138.40, 131.12, 129.66, 128.92, 128.39, 127.89, 124.14, 123.82, 120.37, 57.12, 38.55. (CH_3CN) λ_{max}, nm (ε): 274 (3488), 316 (2949), 302 (2934). Mass ESI$^+$: M^+ = 643.5. Anal. Calcd ($C_{28}H_{26}N_6AuBF_4$) (%). C, 46.05; H, 3.59; N, 11.51. Found: C, 45.92; H, 3.77; N, 11.20.

[AuCu$_2$X$_2$(CH$_3$imCH$_2$quin)$_2$]BF$_4$ (X = Cl, Br, and I) 4−6. X = Cl, 4. A 25 mL round-bottom flask was charged with 0.020 g (0.028 mmol) of [Au(CH_3imCH$_2$quin)$_2$]BF_4 and 5 mL of CH_2Cl_2. To this was added 0.006 g (0.055 mmol) of CuCl·H_2O suspended in 5 mL of CH_2Cl_2. The mixture was stirred at room temperature for 15 min, after which the solution became homogeneous. The solution was stirred for another 6 h during which time a yellow precipitate formed. The solid was collected by filtration yielding 0.019 g (0.020 mmol, 68%). The yellow solid was recrystallized from CH_3CN and diethyl ether to produce yellow crystals. ^{1}H NMR (400 MHz, CD_3CN, 25 °C) same as **3**.

X = Br, 5. Made analogously to **4** except CuBr·H_2O was used in place of CuCl·H_2O (50%). ^{1}H NMR (400 MHz, CD_3CN, 25 °C) same as **3**.

X = I, 6. Made analogously to **4** except CuI·H_2O was used in place of CuCl·H_2O (73%). Anal. Calcd ($C_{28}H_{26}N_6AuCu_2I_2BF_4\cdot 2H_2O$) (%). C, 29.31; H, 2.64; N, 7.33. Found: C, 28.77; H, 2.11; N, 6.90. ^{1}H NMR (400 MHz, CD_3CN, 25 °C) same as **3**.

AuCuBr$_2$(CH$_3$imCH$_2$quin)$_2$, 7. Compound **7** was obtained with great difficulty as the byproduct of the reaction of **3** with CuBr. The equimolar reaction mixture was stirred at room temperature for 6 h until a green yellow precipitate formed. The solid was collected by filtration. Recrystallized by dissolving in hot CH_3CN followed by filtering through Celite and reducing to minimum volume. Diethyl ether was slowly added to the concentrated solution of **7** to yield red crystals (13%). ^{1}H NMR (400 MHz, CD_3CN, 25 °C) same as **3**.

[AuCu$_2$X$_2$(CH$_3$imCH$_2$py)$_2$]BF$_4$ (X = Cl, Br, and I) 9−11. X = Cl, 9. A 25 mL round-bottom flask was charged with 0.021 g (0.0317 mmol) of Au(CH_3imCH$_2$py)$_2$$BF_4$ and 5 mL of CH_2Cl_2. To this was added 0.007 g (0.06 mmol) of CuCl·H_2O suspended in 5 mL of CH_2Cl_2. The mixture was stirred at room temperature for 15 min, after which the solution became homogeneous. The solution was stirred for additional 2 h during which a yellow precipitant formed. The solid was collected by filtration yielding 0.021 g (0.028 mmol, 91%). The solid was recrystallized from CH_3CN and diethyl ether to produce yellow crystals. Anal. Calcd ($C_{20}H_{22}N_6AuCu_2Cl_2BF_4$) (%). C, 28.98; H, 2.68; N, 10.15. Found: C, 28.49; H, 2.55; N, 9.56. ^{1}H NMR (400 MHz, CD_3CN, 25 °C) same as **8**.

X = Br, 10. Made analogously to **9** except CuBr·H_2O was used in place of CuCl·H_2O (79%). Anal. Calcd ($C_{20}H_{22}N_6AuCu_2Br_2BF_4\cdot H_2O$) (%). C, 25.67; H, 2.59; N, 8.59. Found: C, 25.43; H, 2.41; N, 8.64. ^{1}H NMR (400 MHz, CD_3CN, 25 °C) same as **8**.

X = I, 11. Made analogously to **9** except CuI was used in place of CuCl·H_2O (64%). Anal. Calcd ($C_{20}H_{22}N_6AuCu_2I_2BF_4$) (%). C, 23.74; H, 2.19; N, 8.33. Found: C, 23.73; H, 2.13; N, 7.97. ^{1}H NMR (400 MHz, CD_3CN, 25 °C) same as **8**.

[AuCu(CH$_3$imCH$_2$py)$_2$(CH$_3$CN)$_2$](BF$_4$)$_2$, 12. A 25 mL round-bottom flask was charged with 0.020 g (0.032 mmol) of [Au(CH_3imCH$_2$py)$_2$]BF_4, 0.010 g (0.032 mmol) of [Cu(CH_3CN)$_4$]BF_4, and 10 mL of CH_3CN. The mixture was stirred for 15 min at room temperature. The volume was subsequently reduced to 5 mL, and a white solid was precipitated with diethyl ether (0.025 g (0.029 mmol, 92%)). The solid was recrystallized from CH_3CN by slow addition of diethyl ether. Anal. Calcd [$C_{20}H_{22}N_6AuCuB_2F_8$] (%). C, 30.74; H, 2.84; N, 10.76. Found: C, 30.75; H, 3.01; N, 10.49. ^{1}H NMR (400 MHz, CD_3CN, 25 °C) same as **8**.

Results

As shown in Scheme 1, the reaction of 2 equiv of [H(CH_3imCH$_2$quin)]BF_4, **1**, with 1 equiv of $AgBF_4$ produces the monometallic [Ag(CH_3imCH$_2$quin)$_2$]BF_4, **2**, in high yield and purity. Additionally, the treatment of **2** with Au(tht)Cl yields the colorless [Au(CH_3imCH$_2$quin)$_2$]BF_4, **3**. Addition of 2 equiv of CuCl·H_2O to this Au(I) complex produces in moderate yields the mixed-metal complex, [$AuCu_2Cl_2$-(CH_3imCH$_2$quin)$_2$]BF_4, **4**, which contains a butterfly Cu_2Cl_2 core. Similarly, addition of 2 equiv of CuBr·H_2O or

Scheme 2

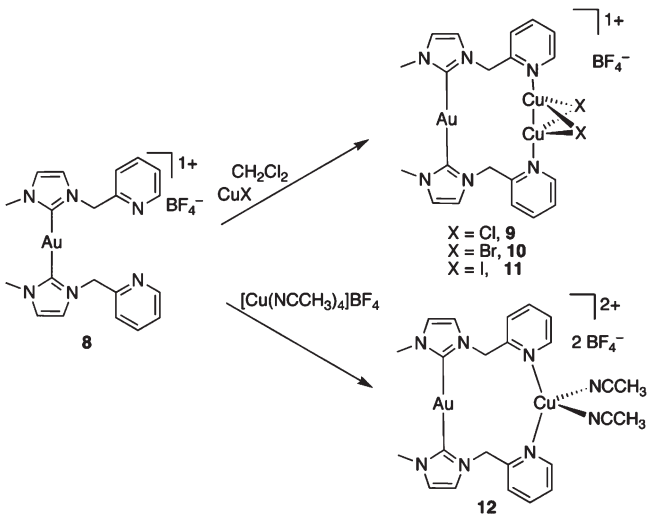

$CuI \cdot H_2O$ to 1 equiv of $[Au(CH_3imCH_2quin)_2]BF_4$ produces the homologous $[AuCu_2Br_2(CH_3imCH_2py)_2]BF_4$, **5**, and $[AuCu_2I_2(CH_3imCH_2py)_2]BF_4$, **6**, in good yields. The Cu(I)-containing $AuCuBr_2(CH_3imCH_2py)_2$, **7**, was first isolated as a byproduct in the reaction to form **5**. Its presence can be enhanced by recrystallization of **5** from hot CH_3CN and slow addition of diethyl ether suggesting that the Cu_2Br_2 cluster dissociates from **5** in acetonitrile solution. Compound **7** can be prepared directly with difficulty and in low yield by the equimolar reaction of **3** with CuBr.

The analogous pyridyl containing species were similarly prepared as shown in Scheme 2. The colorless $[Au(CH_3imCH_2py)_2]BF_4$ reacts with $CuCl \cdot H_2O$ to yield the mixed-metal, $[AuCu_2Cl_2(CH_3imCH_2py)_2]BF_4$, **9**, which like **4**− **6**, contains a butterfly Cu_2X_2 core. Likewise, the analogous reactions with either $CuBr \cdot H_2O$ or $CuI \cdot H_2O$ similarly produce the corresponding multimetallic complexes **10**, $[AuCu_2Br_2(CH_3imCH_2py)_2]BF_4$, or $[AuCu_2I_2(CH_3imCH_2py)_2]BF_4$, **11**. Finally, in the absence of a halide to bridge the copper centers, addition of $[Cu(NCCH_3)_4]BF_4$ to **8** produces the simple dimetallic complex, $[AuCu(NCCH_3)_2(CH_3imCH_2py)_2](BF_4)_2$, **12**.

The carbene precursor, $[H(CH_3imCH_2quin)]BF_4$, and its complexes were studied by ^1H NMR spectroscopy in CD_3CN at 25 °C. The ^1H NMR spectrum of **1** shows 11 resonances with the most downfield resonance at 9.28 ppm, attributed to the imidazolium proton on the carbene carbon. Additionally, six aromatic resonances attributed to the quinolyl group are observed at 8.35, 7.95, 7.77, 7.62, and 7.59 ppm, while the remaining two imidazole backbone resonances appear at 7.57 and 7.42 ppm, respectively. Finally, there are two singlets at 5.74 and 3.91 ppm assigned to the methylene and methyl protons. Upon coordination of Ag(I) to form complex **2** the most downfield resonance disappears, and the methylene and methyl resonances shift upfield to 5.47 ppm and 3.72 ppm, respectively. The remaining eight resonances also shift slightly upfield by ~0.1 ppm. Addition of Au(tht)Cl to **2** in a carbene transfer reaction yields complex **3**, and shifts the methylene and methyl resonances downfield to 5.51 and 3.74 ppm while leaving the aromatic resonances relatively unchanged. Complexes **4**−**7** exhibit ^1H NMR spectra similar to that of complex **3** with little or no apparent change in the quinolyl resonances, indicating that the Cu centers dissociate upon solvation. Lowering the temperature only precipitates the complexes, and no useful spectra could be obtained. The NMR spectra of **8** were described previously,[32] and like the quinolyl analogue, the copper centers in complexes **9**−**12** appear to dissociate in solution rendering the ^1H NMR spectra indistinguishable from that of **8**.

Table 3. Selected Bond Lengths (Å) and Angles (deg) for Complexes **4**−**6**

	4 (X = Cl)	**5** (X = Br)	**6** (X = I)
Cu(1)−Cu(2)	2.903(3)	2.6065(19)	2.546(5)
Au(1)−Cu(1)	3.014(3)	2.9058(17)	2.814(3)
Au(1)−Cu(2)	2.899(3)	2.8533(17)	2.890(3)
Cu(1)−X(1)	2.268(6)	2.418(2)	2.610(4)
Cu(1)−X(2)	2.381(5)	2.388(2)	2.596(4)
Cu(2)−X(1)	2.345(5)	2.418(2)	2.578(4)
Cu(2)−X(2)	2.335(5)	2.445(2)	2.602(4)
Au(1)−C(1)	2.335(5)	2.041(12)	1.94(3)
Au(1)−C(15)	2.052(17)	2.040(12)	1.97(3)
Cu(1)−N(3)	1.974(14)	1.988(9)	2.02(2)
Cu(2)−N(6)	1.979(13)	1.994(9)	1.98(2)
Au(1)−$Cu_{2(centroid)}$	2.58	2.568	2.55
C(1)−N(1)	1.28(2)	1.283(15)	1.33(3)
C(1)−N(2)	1.41(2)	1.367(13)	1.46(3)
C(15)−N(4)	1.30(2)	1.300(15)	1.33(3)
C(15)−N(5)	1.35(2)	1.359(15)	1.44(3)
Cu(1)−Au(1)−Cu(2)	58.78(7)	53.81(4)	53.00(9)
Au(1)−Cu(1)−Cu(2)	58.64(7)	62.06(5)	65.04(11)
Au(1)−Cu(2)−Cu(1)	62.58(8)	64.12(5)	61.95(10)
Cu(1)−X(1)−Cu(2)	77.99(18)	65.24(6)	58.66(11)
Cu(1)−X(2)−Cu(2)	75.97(17)	65.27(6)	58.78(11)
N(3)−Cu(1)−Cu(2)	171.3(5)	172.0(3)	173.8(7)
N(3)−Cu(1)−X(1)	135.9(5)	114.9(3)	113.9(6)
N(3)−Cu(1)−X(2)	123.6(5)	128.9(3)	123.7(7)
N(6)−Cu(2)−Cu(1)	178.2(5)	175.3(3)	174.7(7)
N(6)−Cu(2)−X(1)	131.9(5)	125.5(3)	123.6(6)
N(6)−Cu(2)−X(2)	126.0(5)	119.1(3)	114.2(6)
N(2)−C(4)−C(5)	108.3(15)	112.1(10)	113(2)
N(5)−C(18)−C(19)	113.2(16)	113.9(10)	108(2)
C(1)−Au(1)−C(15)	171.2(8)	177.3(5)	174.6(12)
N(3)−Cu(1)−Cu(2)−N(6)	−10(17)	143(4)	145(9)

Complexes **4**−**7** and **9**−**12** were also studied by X-ray crystallography. Clear, yellow needles of $[AuCu_2Cl_2(CH_3imCH_2quin)_2]BF_4$, **4**, crystallize in the monoclinic space group, $P2(1)/c$, with the cation and the tetrafluoroborate anion residing in the asymmetric unit. Only weakly diffracting crystals (mean $I/\sigma = 1.6$, $2\theta_{max} = 34°$) could be obtained; however, these data are good enough to locate the heavier atoms with certainty. Selected bond lengths and angles are provided in Table 3 while crystallographic data are presented in Table 1. As shown in Figure 1, the cation contains a butterfly Cu_2Cl_2 cluster straddled by the quinolyl groups to one side of the Au center. The Cu(1)−Cu(2) bond at 2.903(3) Å is twisted by ~48° relative to the C(1)−C(15) vector. The Au center is nearly linearly coordinated to the NHC moieties with the C(1)−Au(1)−C(15) angle measuring 171.2(8)°. The two heterometallic separations deviate slightly with Au(1)−Cu(1) and Au(1)−Cu(2) distances of 3.014(3) and 2.899(3) Å. The Au(1)−$Cu_{2(centroid)}$ separation at 2.579 Å places the Cu_2Cl_2 dimer very close to the Au center. The intermetallic angles deviate from equilateral behavior with Cu(1)−Au(1)−Cu(2) at 58.78(7)°, Au(1)−Cu(1)−Cu(2) at 58.64(7)°, and Au(1)−Cu(2)−Cu(1) at 62.58(8)°. The two halides do not evenly bridge the Cu−Cu vector. The Cu(1)−Cl(1) distance at 2.268(6) Å is slightly shorter than the Cu(1)−Cl(2) distance of 2.381(5) Å. Likewise, Cl(2) is slightly distorted toward Cu(1) with the Cu(1)−Cl(2) separation of 2.381(5) Å, which is similar the Cu(2)−Cl(2) separation of 2.335(5) Å. The related Cu(1)−Cl(1)−Cu(2) and

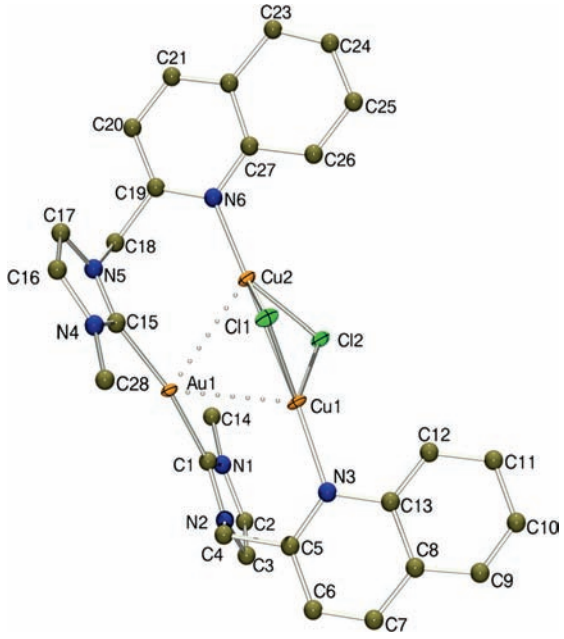

Figure 1. X−ray structural drawing of the cationic portion of $[AuCu_2Cl_2(CH_3imCH_2quin)_2]BF_4$, **4**, with 50% thermal ellipsoids. The carbon and nitrogen atoms are represented by shaded circles. The hydrogen atoms are omitted for clarity.

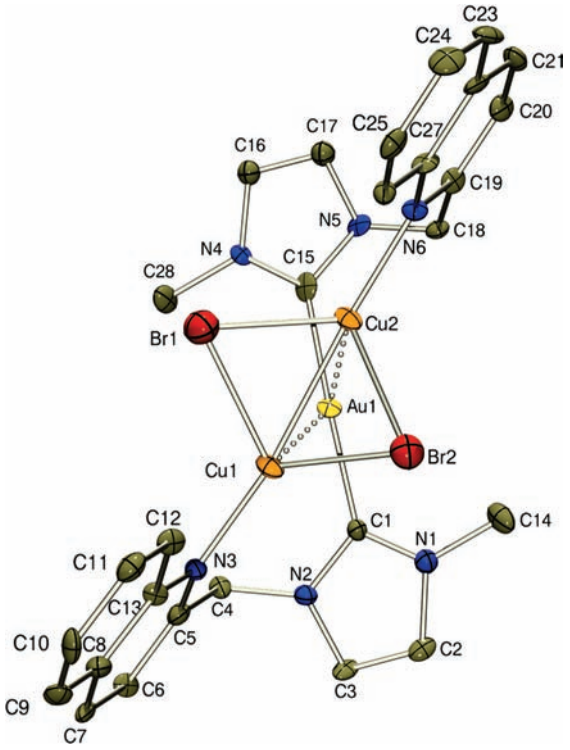

Figure 2. ORTEP drawing of the cationic portion of $[AuCu_2Br_2(CH_3imCH_2quin)_2]BF_4$, **5**, with 50% thermal ellipsoids. Hydrogen atoms omitted for clarity.

Cu(1)−Cl(2)−Cu(2) angles measure 77.99(18) and 75.97(17)°. The Cu_2Cl_2 unit is nearly linearly coordinated to one of the quinolyl nitrogen atoms with Cu(1)−Cu(2)−N-(6) measuring 178.2(5)° while the connection to N(3) is slightly bent with the Cu(2)−Cu(1)−N(3) angle decreased to 171.3(5)°. The Cu−N separations are nearly equal at 1.974(14) and 1.979(13) Å for Cu(1)−N(3) and Cu(2)−N(6), respectively.

High quality crystals of **5**, $[AuCu_2Br_2(CH_3imCH_2$-$quin)_2]BF_4$, form as yellow needles and crystallize in the triclinic space group $P\bar{1}$. The asymmetric unit includes the cation, anion, and one benzonitrile solvate. The selected metrical parameters are provided in Table 3, while the cationic portion of the complex is depicted in Figure 2. Crystallographic data are presented in Table 1. The structure of **5** is similar to that of **4** with a few notable differences. For example, the Au(1)−Cu(1) and Au(1)−Cu(2) distances at 2.9058(17) and 2.8533(17) Å are slightly shorter than those found in **4** while the Cu(1)−Cu(2) separation at 2.6065(19) Å is considerably shorter. Like **4** the Cu_2 unit (Au(1)−$Cu_{2(centroid)}$ = 2.57 Å) is held very close to the Au center and is twisted by 58.45° relative to the C(1)−C(15) vector. These differences are also manifested in the Cu(1)−Au(1)−Cu(2), Au(1)−Cu(1)−Cu(2), and Au(1)−Cu(2)−Cu(1) angles at 53.81(4), 62.06(5), and 64.12(5)°, respectively which are more distorted than those found in **4**. Interestingly, Br(1) is perfectly bridging between Cu(1) and Cu(2) as shown by the identical Cu(1)−Br(1) and Cu(2)−Br(1) bond lengths of 2.418(2) Å while Br(2) is slightly distorted toward Cu(1) with Cu(1)−Br(2) and Cu(2)−Br(2) distances of 2.388(2) and 2.445(2) Å, respectively. The Cu(1)−Br(1)−Cu(2) and Cu-(1)−Br(2)−Cu(2) angles at 65.24(6) and 65.27(6)° are much smaller than those found in **4**. The Cu_2Br_2 unit is less tightly bound to the quinolyl nitrogen atoms with slightly longer Cu(1)−N(3) and Cu(2)−N(6) distances of 1.988(9) and 1.994(9) Å and more uniform Cu(1)−Cu(2)−N(6) and Cu(2)−Cu(1)−N(3) angles of 175.3(3) and 172.0(3)°, respectively. Likewise each imidazole ring is coordinated to the Au(I) center with Au(1)−C(1) and Au(1)−C(15) separations of 2.041(12) and 2.040(12) Å, respectively. The imidazole rings are nearly coplanar with the dihedral angle between the rings measuring only 9.25°, while each imidazole ring is positioned nearly orthogonally to the connected quinolyl moiety. The interplanar angle between the N(1)-containing imidazole ring and N(3)-containing quinolyl ring is 77.8°, while the related angle between the N(4)-containing imidazole ring and the N(6)-containing quinolyl ring is 80.0°. The methylene linkages connecting these groups are slightly strained to accommodate the Cu_2Br_2 species with slightly expanded N(2)−C(4)−C(5) and N(5)−C(18)−C(19) angles of 112.1(10) and 113.9(10)°, respectively.

Similar to **4**, yellow needles of $[AuCu_2I_2(CH_3imCH_2$-$quin)_2]BF_4$, **6**, crystallize in the monoclinic space group $P2(1)/n$ where one cation, one anion, and an acetonitrile solvate in the asymmetric unit. Only weakly diffracting crystals (mean I/σ = 0.83, 2θ max = 31°) could be obtained. However, these data are good enough to locate the heavier atoms with certainty. Selected bond lengths and angles are provided in Table 3 while the cationic unit is presented in Figure 3. Like **4** and **5**, compound **6** contains a nearly linearly coordinated Au(I) center connected to a Cu_2I_2 dimer held in place by the quinolyl ligands. Notably, compound **6** contains the shortest metal−metal separations with Au(1)−Cu(1) and Au(1)−Cu(2) distances of 2.814(3) and 2.890(3) Å, respectively, while the Cu(1)−Cu(2) separation is considerably contracted at 2.546(5) Å. This dimetallic unit is also held very close to the Au(I) with a Au(1)−$Cu_{2(centroid)}$ separation of only 2.55 Å, and this unit is twisted by ~43° relative to the C(1)−C(15) vector. To accommodate the shorted Cu−Cu

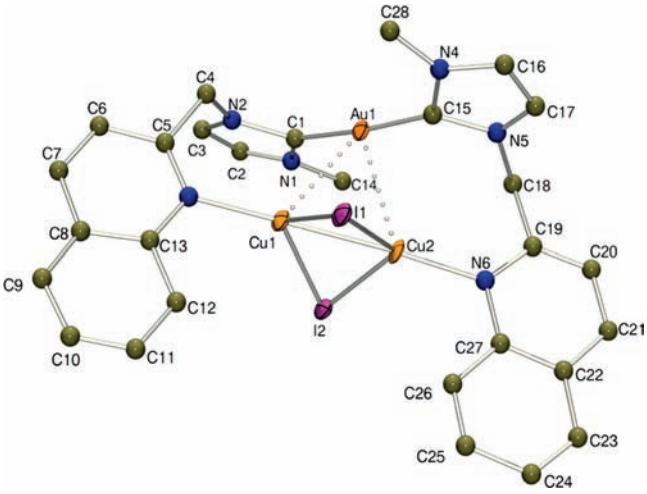

Figure 3. Crystal structure drawing of cationic portion of $[AuCu_2I_2(CH_3imCH_2quin)_2]BF_4$, **6**, with 50% thermal ellipsoids. The carbon and nitrogen atoms are represented by shaded circles while the hydrogen atoms are omitted for clarity.

linkage, the intermetallic angles distort to 53.00(9), 65.04(11), and 61.95(10)° for Cu(1)−Au(1)−Cu(2), Au(1)−Cu(1)−Cu(2), and Au(1)−Cu(2)−Cu(1), respectively. The iodide atoms bridge asymmetrically with Cu(1)−I(1) and Cu(1)−I(2) distances of 2.610(4) and 2.596(4) Å, respectively. The Cu(2)−I(1) and Cu(2)−I(2) separations register 2.578(4) and 2.602(4) Å, respectively. The angles about the bridging iodides are nearly equal with Cu(1)−I(1)−Cu(2) and Cu(1)−I(2)−Cu(2) angles of 58.66(11) and 58.78(11)°, respectively. The Cu_2I_2 unit is attached to the quinolyl nitrogen atoms in a nearly linear fashion with Cu(1)−Cu(2)−N(6) and Cu(2)−Cu(1)−N(3) angles of 174.7(7) and 173.8(7)° and Cu(1)−N(3) and Cu(2)−N(6) distances of 2.02(2) and 1.98(2) Å, respectively. The remaining metrical parameters are not reliable because of poor data.

Red/orange blocks of $AuCuBr_2(CH_3imCH_2quin)_2$, **7**, crystallize in the monoclinic space group $P2(1)/c$. A view of this molecule is presented in Figure 4 while selected bond lengths and angles are shown in Table 4. Crystallographic data are presented in Table 1. The asymmetric unit contains the entire neutral compound that consists of a distorted trigonal planar Cu(I) center interacting with a nearly linearly coordinated Au(I) center. The Au(1)−Cu(1) and N(6)−Cu(1) separations of 2.9581(6) and 2.078(4) Å, are slightly longer than the previous three quinolyl-containing structures. The bonding environment around the Cu(I) center is somewhat irregular with an expanded Br(1)−Cu(1)−Br(2) angle of 132.43(3)° and contracted N(6)−Cu(1)−Br(1) and N(6)−Cu(1)−Br(2) angles of 115.14(11) and 108.55(11)°. The Cu−Br vectors are nearly orthogonal with respect to the Au center with Au(1)−Cu(1)−Br(2) and Au(1)−Cu(1)−Br(1) angles of 94.00(2) and 82.53(2)°, respectively,while the Au(1)−Cu(1)−N(6) angle is expanded to 117.18(11)°. The N(5)−C(18)−C(19) angle around methylene linker is slightly expanded to 114.9(4)° to accommodate the copper center, and this angle is smaller than the corresponding N(2)−C(4)−C(5) angle of 110.6(4)° connecting the uncoordinated quinolyl group. The Cu(1)−Br(1) and Cu(1)−Br(2) bond lengths are 2.3270(8) and 2.3493(8) Å, respectively, and the Cu(I) atom is puckered toward the Au center only 0.254 Å relative to the N(6), Br(1), Br(2)-plane. The Au(I) center is

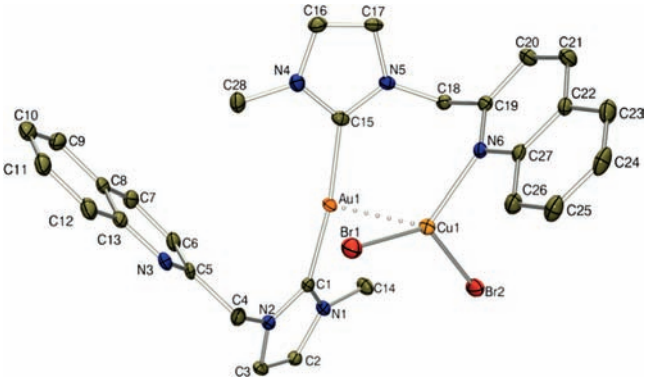

Figure 4. Crystal structure drawing of $AuCuBr_2(CH_3imCH_2quin)_2$,**7**, (50% thermal ellipsoids). Hydrogen atoms are omitted for clarity.

Table 4. Selected Bond Lengths (Å) and Angles (deg) for $AuCuBr_2(CH_3imCH_2quin)_2$, **7**

Cu(1)−Au(1)	2.9581(6)	Au(1)−Cu(1)−Br(1)	82.53(2)
Cu(1)−Br(1)	2.3270(8)	Au(1)−Cu(1)−Br(2)	94.00(2)
Cu(1)−Br(2)	2.3493(8)	Au(1)−Cu(1)−N(6)	117.18(11)
Cu(1)−N(6)	2.078(4)	C(1)−Au(1)−C(15)	171.71(19)
Au(1)−C(1)	2.022(5)	N(6)−Cu(1)−Br(1)	115.14(11)
Au(1)−C(15)	2.025(5)	N(6)−Cu(1)−Br(2)	108.55(11)
C(1)−N(1)	1.347(6)	N(5)−C(18)−C(19)	110.6(4)
C(2)−N(2)	1.355(6)	N(2)−C(4)−C(5)	114.9(4)
C(15)−N(4)	1.344(6)	Br(1)−Cu(1)−Br(2)	132.43(3)
C(15)−N(5)	1.352(6)	N(1)−C(1)−C(15)−N(5)	−46.25

nearly linearly coordinated (C(1)−Au(1)−C(15) = 171.71(19)°) to two imidazole rings which are twisted by 42.06° out of coplanarity from each other. The N(6)-containing quinolyl ring is significantly twisted (80.1°) relative to the N(5)-containing imidazole moiety, and this value is close to the 78.8° angle between the N(3)-containing quinolyl group and the N(2)-containing imidazole plane.

Yellow needles of $[AuCu_2Cl_2(CH_3imCH_2py)_2]BF_4$, **9**, crystallize in the triclinic space group $P\bar{1}$, with one cation and one slightly disordered tetrafluoroborate anion in the asymmetric unit. Crystallographic data are presented in Table 2 while selected bond angles and lengths are provided in Table 5. As shown in Figure 5, the overall structure of **9** is very similar to that of **4** with a nearly linearly coordinated Au(I)-center bound to a Cu_2Cl_2 cluster held in place by the picolyl groups. The Au(1)−Cu(1) and Au(1)−Cu(2) separations measure 2.9097(5) and 2.8655(5) Å while the Cu(1)−Cu(2) separation is 2.7063(7) Å. Like the quinolyl species the Au(1)−$Cu_{2(centroid)}$ distance in **9** is short at 2.55 Å. The Cu_2Cl_2 unit is not symmetrically positioned relative to the Au(I) center as evidenced by the variance in the Cu(1)−Au(1)−Cu(2), Au(1)−Cu(1)−Cu(2), and Au(1)−Cu(2)−Cu(1) intermetallic angles of 55.973(14), 61.020(15), and 63.007(15)°, respectively. Moreover, this Cu_2 unit is twisted by 68.82° relative to the C(1)−C(15) vector. The Cu(1)−Cl(1) and Cu(1)−Cl(2) separations at 2.4059(10) and 2.2547(9) Å differ from each other, as do the Cu(2)−Cl(1) and Cu(2)−Cl(2) distances which measure 2.2694(9) and 2.4582(10) Å, respectively. Despite the asymmetric halide coordination, the Cu(1)−Cl(1)−Cu(2) and Cu(1)−Cl(2)−Cu(2) angles at 70.67(3) and 69.94(3)°, respectively, only slightly deviate from each other. The Cu_2 unit does not linearly coordinate to the two picolyl groups as shown by the corresponding N(3)−Cu(1)−Cu(2) and N(6)−Cu(2)−Cu(1) angles of 163.20(9) and 158.18(9)°, respectively. The N(3)−Cu(1) and N(6)−Cu(2) bond lengths at 1.972(3)

Table 5. Selected Bond Lengths (Å) and Angles (deg) for Complexes **8**–**10**

	9 (X = Cl)	**10** (X = Br)	**11** (X = I)
Cu(1)–Cu(2)	2.7063(7)	2.6171(6)	2.478(2)
Au(1)–Cu(1)	2.9097(5)	2.8720(5)	2.8368(19)
Au(1)–Cu(2)	2.8655(5)	2.8439(5)	2.8971(19)
Cu(1)–X(1)	2.4059(10)	2.4741(6)	2.613(2)
Cu(1)–X(2)	2.2547(9)	2.4046(5)	2.559(2)
Cu(2)–X(1)	2.2694(9)	2.4205(5)	2.566(2)
Cu(2)–X(2)	2.4582(10)	2.4857(6)	2.625(2)
Au(1)–C(1)	2.017(4)	2.025(3)	1.985(15)
Au(1)–C(11)	2.021(4)	2.026(3)	2.016(16)
Cu(1)–N(3)	1.972(3)	1.985(3)	1.986(10)
Cu(2)–N(6)	1.970(2)	1.981(3)	1.983(11)
Au(1)–Cu(centroid)	2.546	2.541	2.586
Cu(1)–Au(1)–Cu(2)	55.973(14)	54.496(12)	51.19(5)
Au(1)–Cu(1)–Cu(2)	61.020(15)	62.204(14)	65.66(6)
Au(1)–Cu(2)–Cu(1)	63.007(15)	63.300(14)	63.15(6)
Cu(1)–X(1)–Cu(2)	70.67(3)	64.635(17)	57.15(6)
Cu(1)–X(2)–Cu(2)	69.94(3)	64.684(16)	57.08(6)
N(3)–Cu(1)–Cu(2)	163.20(9)	171.22(8)	167.7(3)
N(3)–Cu(1)–X(1)	112.01(9)	115.08(8)	107.3(3)
N(3)–Cu(1)–X(2)	137.22(9)	128.92(8)	127.5(3)
N(6)–Cu(2)–Cu(1)	158.18(9)	168.10(8)	172.0(3)
N(6)–Cu(2)–X(1)	142.91(10)	132.32(8)	124.2(3)
N(6)–Cu(2)–X(2)	107.80(9)	112.72(8)	111.9(3)
N(2)–C(4)–C(5)	109.8(3)	110.2(3)	113.9(13)
N(5)–C(14)–C(15)	112.9(3)	113.0(3)	110.6(13)
C(1)–Au(1)–C(11)	177.16(14)	175.99(13)	175.9(6)
N(3)–Cu(1)–Cu(2)–N(6)	−177.3(4)	179.7(7)	−158(4)

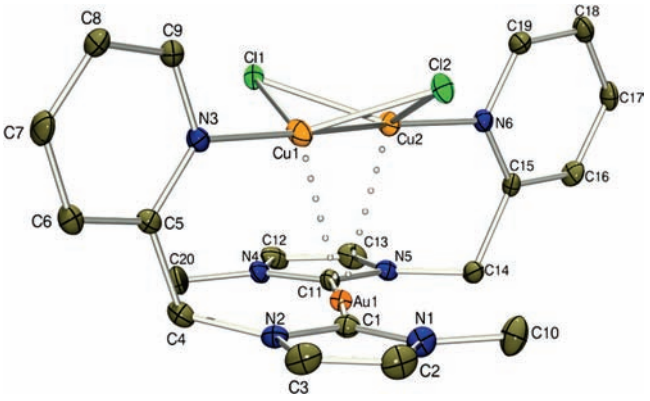

Figure 5. X-ray crystal structure of the cationic portion shown with 50% thermal ellipsoids of $[AuCu_2Cl_2(CH_3imCH_2py)_2]BF_4$, **9**. Hydrogen atoms omitted for clarity.

and 1.970(3) Å, respectively, are similar to those in the related quinolyl complex **4**. Also similar is the coordination about the Au(I) center where the C(1)–Au(1)–C(11) angle registers 177.16(14)°, and the Au(1)–C(1) and Au(1)–C(11) distances measure 2.017(4) and 2.021(4) Å, respectively. The two imidazole groups are nearly coplanar with a dihedral angle of only 4.23°. Likewise, the two pyridyl rings are similarly distorted out of plane from one another by 5.82° while the pyridyl-imidazole interplanar angles are nearly orthogonal with an 87.5° angle between the N(3)-containing pyridyl group and the N(2)-containing imidazole ring and an 81.1° angle between the N(6)-containing pyridyl ring and the N(5)-containing imidazole moiety.

Yellow crystals of $[AuCu_2Br_2(CH_3imCH_2py)_2]BF_4$, **10**, also crystallize in the triclinic space group $P\bar{1}$ with only one cation and one anion in the asymmetric unit. Crystallographic data are presented in Table 2 while Figure 6 presents a structural drawing of the cationic portion of the molecule.

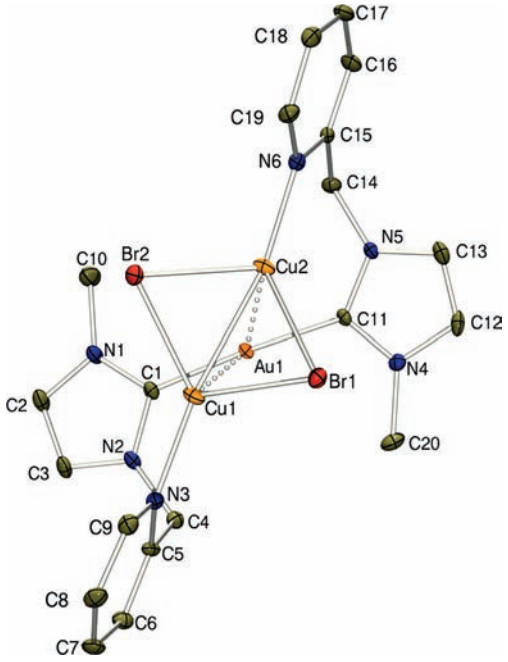

Figure 6. ORTEP structural drawing of the cationic portion of **10**, $[AuCu_2Br_2(CH_3imCH_2py)_2]BF_4$. (50% thermal ellipsoids) Hydrogen atoms are omitted for clarity.

Selected bond distances and angles are presented in Table 5. The structure of **10** is very similar to that of **9** with some notable differences in the metrical parameters about the metal centers. The Au(1)–Cu(1) and Au(1)–Cu(2) distances at 2.8720(5) and 2.8439(5) Å are only slightly shorter than the corresponding parameters in **9**; however, in contrast, the Cu(1)–Cu(2) separation shortens significantly to 2.6171(6) Å. Likewise, the Cu_2 dimer is twisted by 72.35° relative to the C(1)–C(15) vector. There is very little change in proximity of the Cu_2 dimer to the Au center with the Au(1)–$Cu_{2(centroid)}$ separation at 2.55 Å. Additionally, the Cu(1)–Au(1)–Cu(2), Au(1)–Cu(1)–Cu(2), and Au(1)–Cu(2)–Cu(1) angles (54.496(12), 62.204(14), and 63.300(14)) are very similar to those found in **9**. The Cu(1)–Br(1) and Cu(1)–Br(2) separations of 2.4741(6) and 2.4046(5) Å are similar to the Cu(2)–Br(1) and Cu(2)–Br(2) separations of 2.4205(5) and 2.4857(6) Å, respectively. The Cu(1)–Br(1)–Cu(2) and Cu(1)–Br(2)–Cu(2) angles are very close at 64.635(17) and 64.684(16)°. Following the trend established in the quinolyl compounds, the Cu(1)–N(3) and Cu(2)–N(6) separations lengthen to 1.985(3) and 1.981(3) Å relative to its chloro-analogue. The N(3)–Cu(1)–Cu(2) and N(6)–Cu(2)–Cu(1) angles (171.22(8) and 168.10(8)°) more closely approach linearity compared to those found in **9**. The remaining geometrical parameters including the coordination environment about the Au(I) center are very similar to those in **9**.

Yellow crystals of $[AuCu_2I_2(CH_3imCH_2py)_2]BF_4$, **11**, form in the monoclinic space group $C2/c$ where the cation, a slightly disordered tetrafluoroborate anion, and fractions of water and diethyl ether solvates are situated in the asymmetric unit. Selected bond lengths and angles are given in Table 5 while crystallographic data are presented in Table 2. As shown in Figure 7, the structure of complex **11** is similar to those of **9** and **10** with some notable differences. The Cu(1)–Cu(2) distance at 2.478(2) Å in **11** is considerably shorter

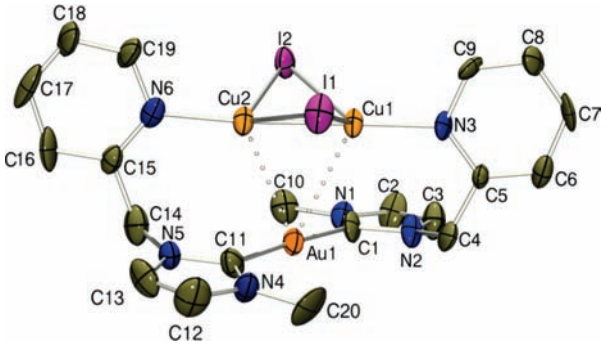

Figure 7. Crystal structure drawing of cationic portion of $[AuCu_2I_2(CH_3imCH_2py)_2]BF_4$, **11** with 50% thermal ellipsoids. The hydrogen atoms are omitted for clarity.

Table 6. Selected Bond Lengths (Å) and Angles (deg) for Complex **12**

Au(1)···Cu(1)	4.732	C(1)−Au(1)−C(11)	177.4(3)
Au(1)−C(1)	2.005(7)	N(6)−Cu(1)−N(3)	119.3(2)
Au(1)−C(11)	2.017(7)	N(3)−Cu(1)−N(7)	100.1(2)
Cu(1)−N(3)	2.051(6)	N(3)−Cu(1)−N(8)	110.9(3)
Cu(1)−N(6)	2.033(5)	N(6)−Cu(1)−N(7)	104.8(2)
Cu(1)−N(7)	2.039(6)	N(6)−Cu(1)−N(8)	112.1(2)
Cu(1)−N(8)	1.963(7)	N(7)−Cu(1)−N(8)	108.2(2)
N(7)−C(21)	1.119(8)	N(2)−C(4)−C(5)	112.5(5)
N(8)−C(23)	1.136(8)	N(5)−C(14)−C(15)	112.9(5)

than the corresponding separations in **9** and **10**, while the intermetallic Au(1)−Cu(1) and Au(1)−Cu(2) separations of 2.8368(19) and 2.88971(19) Å are very similar. Like the quinolyl complex, the Cu_2I_2 dimer is less twisted (39.25°) relative to the C(1)−C(11) vector, and the Au(1)−$Cu_{2(centroid)}$ is slightly longer at 2.59 Å than its chloro- and bromo-analogues. The angles within the triangular core are acute with Cu(1)−Au(1)−Cu(2), Au(1)−Cu(1)−Cu(2), and Au(1)−Cu(2)−Cu(1) angles measuring 51.19(5), 65.66(6), and 63.15(6)°, respectively. The Cu(1)−I(1) and Cu(1)−I(2) separations measure 2.613(2) and 2.559(2) Å which are similar to the Cu(2)−I(1) and Cu(2)−I(2) distances of 2.566(2) and 2.625(2) Å. The angles around these iodide ligands are very similar with the Cu(1)−I(1)−Cu(2) and Cu(1)−I(2)−Cu(2) angles measuring 57.15(6) and 57.08(6)°. The dimetallic unit is not linearly connected to the pyridyl nitrogen atoms as evidenced by the Cu(1)−Cu(2)−N(6) and Cu(2)−Cu(1)−N(3) angles of 172.0(3) and 167.7(3)°. The Cu−N connections in **11** are also lengthened relative to those in **9** with Cu(1)−N(3) and Cu(2)−N(6) separations measuring 1.986(10) and 1.983(11) Å, respectively, and these values are nearly identical to those observed in **10**.

The colorless needles of the halide-free $[Au(CH_3imCH_2py)_2Cu(NCCH_3)_2](BF_4)_2$, **12**, crystallize in the monoclinic space group $P2_1/c$ with two tetrafluoroborate anions, one cation, and an acetonitrile solvent in the asymmetric unit. Selected metrical parameters are provided in Table 6 while crystallographic data are presented in Table 2. As shown in Figure 8, in the absence of halides to form a Cu_2X_2 unit, the cationic Cu(I) center distorts away from the Au(I) center with a long intermetallic separation of 4.732 Å. The Au(I) center is nearly linearly coordinated with the C(1)−Au(1)−C(11) bond angle of 177.4(3)° while the Cu(I) center adopts a slightly distorted tetrahedral geometry composed of two pyridyl rings and two acetonitrile molecules. The N(3)−Cu(1)−N(6) and N(7)−Cu(1)−N(8) angles are 119.3(2) and

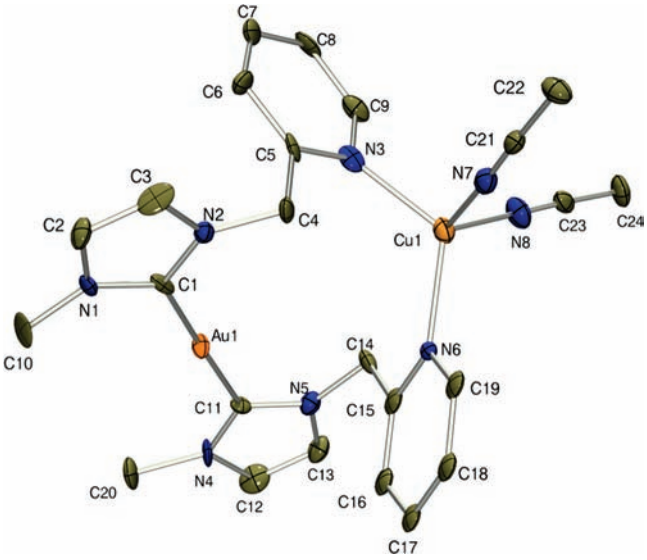

Figure 8. Crystal structural diagram of the cationic portion of $[AuCu(CH_3imCH_2py)_2](BF_4)_2$, **12**, shown with 50% ellipsoids and hydrogen atoms removed for clarity.

108.2(2)° while the N(3)−Cu(1)−N(7) and N(6)−Cu(1)−N(8) angles are 100.1(2) and 112.1(2)°, respectively. The Cu(1)-pyridyl separations are very uniform with Cu(1)−N(3) and Cu(1)−N(6) bond distances of 2.051(6) and 2.033(5) Å while the acetonitrile connections vary slightly with Cu(1)−N(7) and Cu(1)−N(8) measuring 2.039(6) and 1.963(7) Å, respectively. The angles around the methylene linkages are slightly expanded to accommodate the Cu(I) center (112.5(5) and 112.9(5)° for N(2)−C(4)−C(5) and N(5)−C(14)−C(15), respectively), yet there is very little twist (5.66°) between the two imidazole planes.

As indicated by the ^{1}H NMR spectroscopy, the copper containing species are dynamic in solution. To probe the solution dynamics samples of $[AuCu_2Cl_2(CH_3imCH_2py)_2]BF_4$ and $[AuCu_2X_2(CH_3imCH_2quin)_2]BF_4$ (where X = Cl and Br) were analyzed by Cu K-edge X-ray absorption spectroscopy (XAS) in both the solid and solution (CH_3CN) states. Owing to the low solubility of both $[AuCu_2I_2(CH_3imCH_2py)_2]BF_4$ and $[AuCu_2I_2(CH_3imCH_2quin)_2]BF_4$, we were unable to obtain solution X-ray absorption spectra of these compounds of sufficient quality to perform even low resolution EXAFS analyses (the maximum concentrations obtained for these compounds were ~0.2 mM). Therefore, both $[AuCu_2I_2(CH_3imCH_2py)_2]BF_4$ and $[AuCu_2I_2(CH_3imCH_2quin)_2]BF_4$ were not analyzed by XAS in this study. EXAFS spectra of $[AuCu_2Br_2(CH_3imCH_2py)_2]BF_4$ and $[AuCu_2Br_2(CH_3imCH_2quin)_2]BF_4$ were obtained at higher resolution than either $[AuCu_2Cl_2(CH_3imCH_2py)_2]BF_4$ or $[AuCu_2Cl_2(CH_3imCH_2quin)_2]BF_4$. This is due to the gradual and unavoidable photodecomposition of both $[AuCu_2Cl_2(CH_3imCH_2py)_2]BF_4$ and $[AuCu_2Cl_2(CH_3imCH_2quin)_2]BF_4$ in the X-ray beam. Therefore, we were only able to analyze the EXAFS region of the Cu K-edge XAS for $[AuCu_2Cl_2(CH_3imCH_2py)_2]BF_4$ and $[AuCu_2Cl_2(CH_3imCH_2quin)_2]BF_4$ out to k = 12.0 Å^{-1} versus 14.5 Å^{-1} for $[AuCu_2Br_2(CH_3imCH_2py)_2]BF_4$ and $[AuCu_2Br_2(CH_3imCH_2quin)_2]BF_4$.

In both the solution and the solid states the XANES region of the Cu K-edge X-ray absorption spectra for

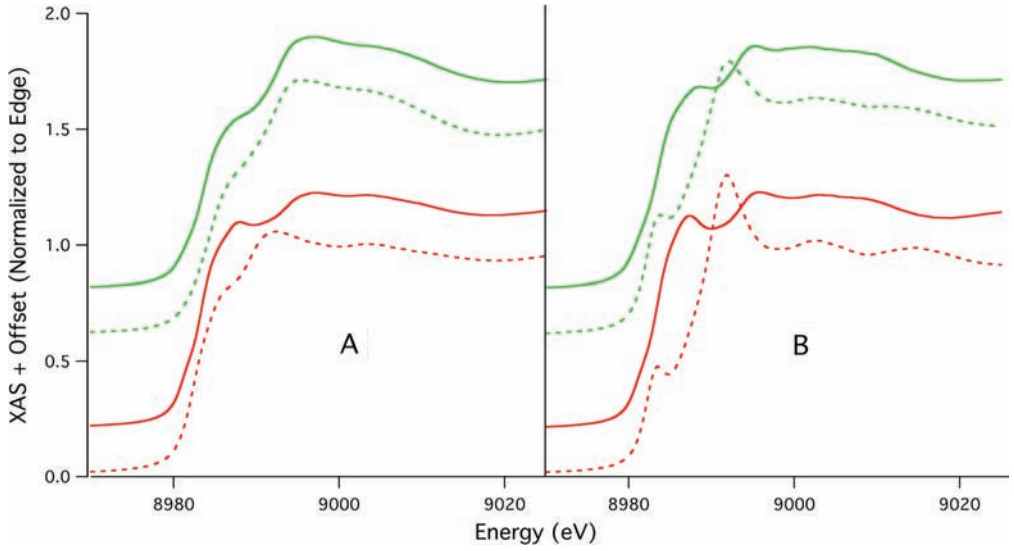

Figure 9. XANES region of the X-ray absorption spectra for $[AuCu_2X_2(CH_3imCH_2py)_2]BF_4$ (A) and $[AuCu_2X_2(CH_3imCH_2quin)_2]BF_4$ (B). The chloride structures are presented in green, and the bromide structures are presented in red. Spectra of the dispersed solids are presented as the solid lines, while the CH_3CN solution spectra are given as the dashed lines.

Scheme 3

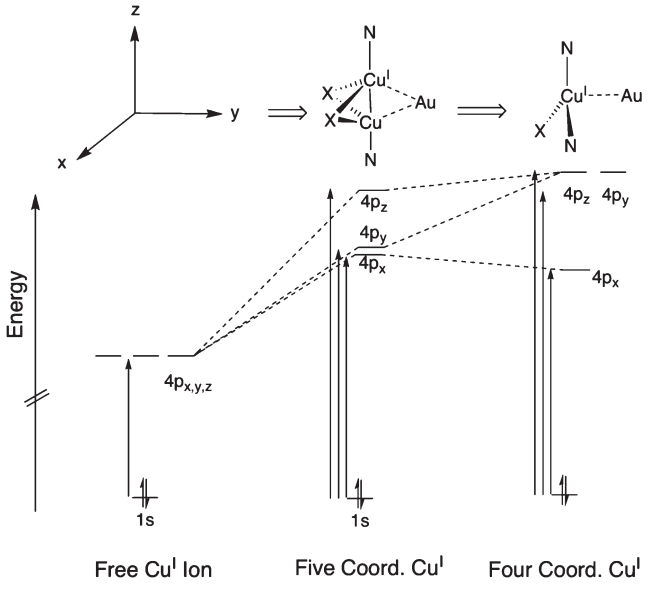

$[AuCu_2X_2(CH_3imCH_2py)_2]BF_4$ and $[AuCu_2X_2(CH_3imCH_2quin)_2]BF_4$ (X = Cl and Br) are typical for Cu^I complexes (Figure 9). The XANES spectra for the solid states are marked by a transition at ~8981 eV that is barely resolvable from the edge and a more prominent feature at ~8984 eV. We assign these two features as the Cu(1s → $4p_x$)/Cu(1s → $4p_y$) and Cu(1s → $4p_z$) transitions, with the lower energy feature being assigned to the former and the higher energy feature to the latter two transitions (Scheme 3). This splitting of the 4p orbitals is to be expected in the highly distorted trigonal bipyramidal ligand environment present in these complexes. The solution spectra obtained for $[AuCu_2Br_2(CH_3imCH_2py)_2]BF_4$ and $[AuCu_2Cl_2(CH_3imCH_2py)_2]BF_4$ are similar to what was observed in the solid state suggestive of a similar coordination geometry about Cu^I in solution (i.e., five coordinate Cu^I). In contrast, the solution spectra of $[AuCu_2Br_2(CH_3imCH_2quin)_2]BF_4$ and $[AuCu_2Cl_2(CH_3imCH_2quin)_2]BF_4$ are indicative of significant change in coordination geometry about the Cu^I centers upon

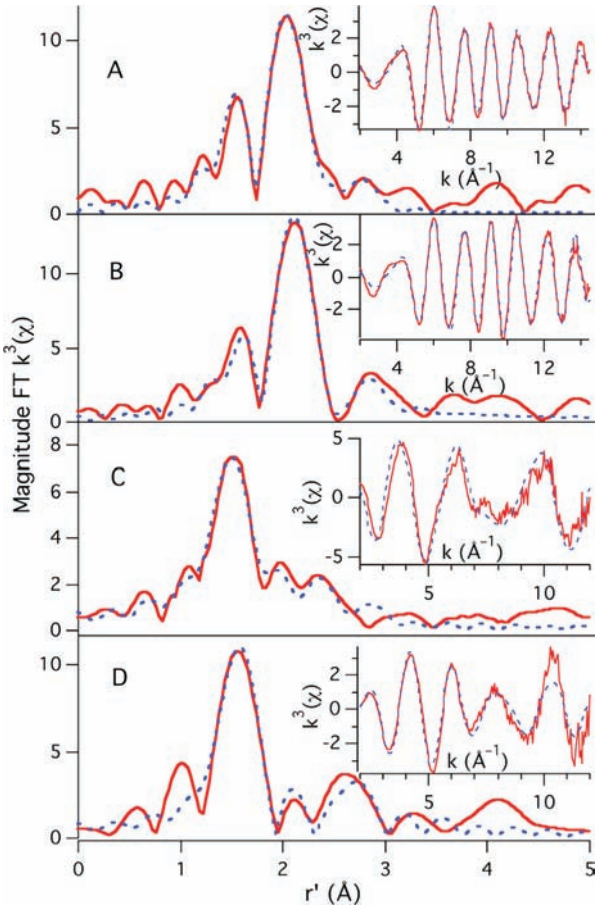

Figure 10. FT $k^3(\chi)$ for the solid state spectra of (A) $[AuCu_2Br_2(CH_3imCH_2py)_2]BF_4$, (B) $[AuCu_2Br_2(CH_3imCH_2quin)_2]BF_4$, (C) $[AuCu_2Cl_2(CH_3imCH_2py)_2]BF_4$, and (D) $AuCu_2Cl_2(CH_3imCH_2quin)_2]BF_4$. The insets depict the corresponding unfiltered $k^3(\chi)$ data. The data are presented as the solid red lines, and the best fits to the data are presented as the dashed blue lines.

Table 7. EXAFS Refinement Parameters for $[AuCu_2X_2(CH_3imCH_2py)_2]BF_4$ and $[AuCu_2X_2(CH_3imCH_2quin)_2]BF_4$ in CH_3CN and in the Solid State

shell	$[AuCu_2Cl_2(CH_3imCH_2py)_2]BF_4$	$[AuCu_2Br_2(CH_3imCH_2py)_2]BF_4$	$[AuCu_2Cl_2(CH_3imCH_2quin)_2]BF_4$	$[AuCu_2Br_2(CH_3imCH_2quin)_2]BF_4$
		Solid		
Pre-edge				
Peak 1	8981.6(3)	8981.2(2)	8981.2(2)	8981.3(2)
Peak 2	8984.3(2)	8983.6(1)	8984.5(3)	8984.3(1)
E_o (eV)[a]	8981.9	8982.2	8986.8	8982.0
N				
n	1	1	1	1
r (Å)	1.955(3)	1.990(3)	1.982(14)	1.992(7)
σ^2 (Å^2)	0.0023(4)	0.0010(3)	0.0008(10)	0.0037(8)
X^-	Cl^-	Br^-	Cl^-	Br^-
n	2	2	2	2
r (Å)	2.24(1)	2.398(3)	2.30(1)	2.408(5)
σ^2 (Å^2)	0.0088(10)	0.0085(4)	0.0022(6)	0.0093(13)
Cu				
n	1	1	1	1
r (Å)	2.77(2)	2.668(9)	2.74(1)	2.658(7)
σ^2 (Å^2)	0.009(2)	0.0061(4)	0.008(1)	0.0028(4)
Au				
n	1	1	1	1
r (Å)	2.9(1)	2.95(2)	2.9(2)	2.94(2)
σ^2 (Å^2)	0.009(1)	0.0073(11)	0.010(2)	0.0066(12)
GOF	0.54	0.38	0.99	0.40
		CH_3CN		
Pre-edge				
Peak 1	8981.2(8)	8981.9(3)	8983.4(1)	8983.5(1)
Peak 2	8987.4(4)	8985.6(4)	8989.6(1)	8989.8(1)
E_o (eV)[a]	8982.0	8982.0	8986.5	8983.1
N				
n	1	1	2	2
r (Å)	1.870(5)	1.911(7)	2.000(8)	1.971(8)
σ^2 (Å^2)	0.0031(6)	0.0033(8)	0.0029(9)	0.0031(10)
N				
n	2	2		
r (Å)	1.951(3)	2.007(4)		
σ^2 (Å^2)	0.005(3)	0.0054(5)		
X^-	Cl^-	Br^-	Cl^-	Br^-
n	1	1	1	1
r (Å)	2.222(6)	2.484(3)	2.26(1)	2.43(2)
σ^2 (Å^2)	0.0096(10)	0.0069(3)	0.0025(11)	0.0012(3)
Au				
n	1	1	1	1
r (Å)	2.93(9)	2.99(1)	3.05(3)	3.06(2)
σ^2 (Å^2)	0.0093(10)	0.0066(13)	0.007(2)	0.001(3)
GOF	0.60	0.47	0.68	0.57

[a] Energy at which EXAFS begins. This was set as a free parameter for the halide shell and then restrained for all other shells to the value of the halide shell.

dissolution; there are two well-defined pre-edge features at ~8983 and 8990 eV, which are assigned as Cu(1s → $4p_x$) and Cu(1s → $4p_{y/z}$) transitions. Such edge features are consistent with distorted 4-coordinate or trigonal planar coordination about Cu, and would thus be consistent with the loss of a ligand to the Cu^I−center (i.e., a Cu^IL_3 complex with a long-range Au-interaction; Scheme 3). Analysis of the EXAFS region of the X-ray absorption spectra is consistent with this change in coordination geometry.

The EXAFS region of the solid-state X-ray absorption spectra for the four complexes are consistent with their X-ray crystal structures (Figure 10, Table 7). For both $[AuCu_2X_2(CH_3imCH_2py)_2]BF_4$ and $[AuCu_2X_2(CH_3imCH_2quin)_2]BF_4$ we find an elongation of the average Cu−N bond length by ~0.02−0.05 Å as Cl^- is replaced with Br^-compensated for by a subsequent shortening of the Cu−Cu bond length by ~0.1 Å. In all cases we find that the average Cu−Au bond length is invariant with changes to both the ligand and the halide. However, we note that the Cu−Au vector at nearly 3.0 Å was difficult to reliably separate from the contributions from the inner-sphere halides, Cu, and the other outer-sphere scatterers.

Upon dissolution in CH_3CN an EXAFS analysis indicates that all four complexes lose one Cu-halide interaction and the Cu−Cu interaction (Figure 11 and Table 7). For $[AuCu_2Br_2(CH_3imCH_2py)_2]BF_4$ and $[AuCu_2Cl_2(CH_3imCH_2py)_2]BF_4$ we find that the EXAFS is best modeled with

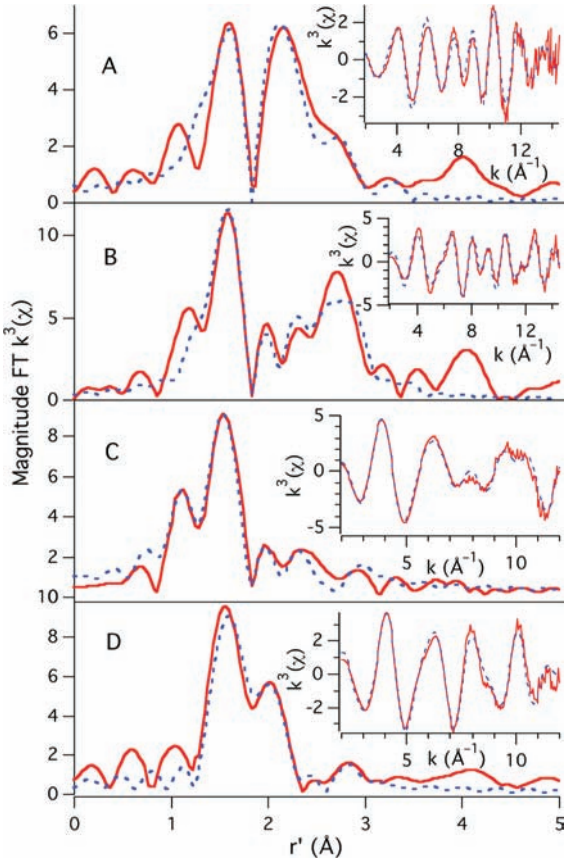

Figure 11. FT $k^3(\chi)$ for the CH_3CN solution spectra of (A) $[AuCu_2Br_2(CH_3imCH_2py)_2]BF_4$, (B) $[AuCu_2Br_2(CH_3imCH_2quin)_2]BF_4$, (C) $[AuCu_2Cl_2(CH_3imCH_2py)_2]BF_4$, and (D) $[AuCu_2Cl_2(CH_3imCH_2quin)_2]BF_4$. The insets depict the corresponding unfiltered $k^3(\chi)$ data. The data are presented as the solid red lines, and the best fits to the data are presented as the dashed blue lines.

one Cu-X interaction (at 2.22 Å for the Cu−Cl bond and 2.48 Å for the Cu−Br bond), one Cu−Au interaction (at ∼2.9 Å in both cases), two Cu−N interactions (at 1.95 Å for $[AuCu_2Cl_2(CH_3imCH_2py)_2]BF_4$ and 2.00 Å for $[AuCu_2Br_2(CH_3imCH_2py)_2]BF_4$), and one short Cu−N interaction at ∼1.9 Å. In contrast, the EXAFS region for the solution spectra of both $[AuCu_2Br_2(CH_3imCH_2quin)_2]BF_4$ and $[AuCu_2Cl_2(CH_3imCH_2quin)_2]BF_4$ were best modeled with one Cu-X interaction (at 2.26 Å for the Cu−Cl bond and 2.43 Å for the Cu−Br bond), one Cu−Au interaction (at ∼3.1 Å in both cases), and two Cu−N interactions at ∼2.0 Å. These fits are consistent with the XANES data; in solution the complexes containing the picolyl moiety maintain a distorted trigonal bipyramidal coordination environment about Cu^I while the complexes containing the sterically more bulky quinolyl moiety have Cu^I contained in a distorted four-coordinate ligand environment.

In acetonitrile the electronic absorption spectra for $[Ag(CH_3imCH_2quin)_2]BF_4$ and $[Au(CH_3imCH_2quin)_2]BF_4$ are nearly identical to that of the ligand precursor, $[CH_3imCH_2quin]BF_4$ with $\pi-\pi^*$ transitions between 270 and 320 nm. Because of the dynamic nature of the copper containing complexes in solution, the electronic absorption spectra for complexes **4**−**7** are almost identical to that of $[Au(CH_3imCH_2quin)_2]BF_4$. Likewise, in acetonitrile, the absorption spectra of **9**−**12** closely resemble that of $[Au(CH_3imCH_2py)_2]BF_4$. All of the complexes are highly luminescent in the solid-state, while in solution they are only weakly emissive as are **3** and **8**.

The quinolyl-ligand precursor, **1**, shows a structured emission spectrum with peaks at 420 and 435 nm with a shoulder appearing at 472 nm when excited at 378 nm. The gold containing complex **3** is highly emissive with one band at 612 nm originating from an excitation at 420 nm. In the solid state the $[AuCu_2X_2(CH_3imCH_2quin)_2]BF_4$ complexes exhibit similar emission spectra consisting of a broad emission bands centered at 550 nm for **4** (X = Cl), 535 nm for **5** (X = Br), and 583 nm for **6** (X = I) when excited at 382 nm. The solid state emission structure of the dimetallic species, $AuCuBr_2(CH_3imCH_2quin)_2$,**7**, is considerably red-shifted with respect to the rest of complexes, and exhibits an emission band at 642 nm. The emission spectra for the picolyl substituted complexes, $[AuCu_2X_2(CH_3imCH_2py)_2]BF_4$ (X = Cl, Br, I) differ slightly relative to the quinolyl analogues. The emission spectra for **9**−**11** have maxima at 545, 554, and 556 nm (λ_{exi} = 382 nm), while the halide free complex **12** shows a much different spectrum with an intense emission observed blue-shifted to 496 nm.

Discussion

The complexes reported here are slightly photosensitive but are air and moisture stable for weeks. The methylene linker between the imidazole and the pyridyl or quinolyl moieties provides enough added flexibility to accommodate the multimetallic butterfly core found in complexes **4**−**6** and **9**−**11**. While there are numerous examples of halide-bridged, copper clusters in the literature,[40] no examples of a halide-bridged, copper dimer in close proximity to a dissimilar metal could be found in the Cambridge Crystallographic Database. In this light, the short separations of ∼2.5 Å between the $Cu_{2(centroid)}$ and the Au(I) center are even more significant. A similar short interaction was observed between a mercurous dimer and a d^{10} center in the loosely related metallocryptand, $[M_2Hg_2(P_2phen)_3]^{2+}$ where M is Pt(0) or Pd(0) and P_2phen is 2,9-bis(diphenylphosphino)-1,10-phenanthroline.[41] In the absence of the halide bridges about the copper dimer, the metal−metal interactions appear repulsive as observed by the long Cu−Au separation of 4.732 Å in complex **12**.

Also interesting is the significant lengthening of the Cu−Cu distance according to halide substitution (Cl < Br < I). The origin of this effect may be attributed to simple hard/soft acid/base interactions where the metal−metal separations decrease at the expense of favorable copper-halide interactions. Accordingly, the longest (weakest) Cu−Cu interaction is found in the chloro-complexes where the hard/hard metal-halide interactions are maximized. Pyykkö and Mendizabal[42] have reproduced this trend, along with the decrease in the Cu−X−Cu angles (Cl > Br > I), theoretically and suggest that the shortened Cu−Cu separations found in the iodo- and bromo-complexes may be attributed to an increased metallophilic attraction. Early work by Subramanian and Hoffmann[43] describing the bonding in halocuprates also presents a similar trend. There are

(40) Jagner, S.; Helgesson, G. *Adv. Inorg. Chem.* **1991**, *37*, 1.
(41) Catalano, V. J.; Malwitz, M. A.; Noll, B. C. *Inorg. Chem.* **2002**, *41*, 6553.
(42) Pyykkö, P.; Mendizabal, F. *Inorg. Chem.* **1998**, *37*, 3018.
(43) Subramanian, L.; Hoffmann, R. *Inorg. Chem.* **1992**, *31*, 1021.

other examples in the literature;[40] however, it is difficult to find an isomorphous series containing an imine ligand trans to the metal−metal bond. For example, White and co-workers[44] observed a very slight lengthening of the Cu−Cu distance from 3.024(2) to 3.097(1) Å in the dimeric [CuX(2,9-dimethyl-1,1-phenanthroline)]$_2$ upon substitution of iodide to bromide. Likewise, Oshido et al.[45] observed a more substantial lengthening from 2.6869(8) to 2.7357(8) Å in the imino-nitroxide complexes, [CuX(immepy)]$_2$ where X is I or Br, respectively. However, as shown by White and co-workers,[46] when steric encumbrance around the copper centers becomes important, these electronic effects can be negated.

The short Cu−Cu separations observed here, particularly in the bridging iodide complexes, are not unprecedented. For example, Cu···Cu separations of 2.69 Å are found in the simple copper(I) clusters such as $Cu_4Br_4(py)_4$.[24] Additionally, Fu and co-workers reported a di-μ-iodo-bis({2-(diphenylphosphoryl)methyl-amino]-7-methyl-1,8-naphthyridine-κN^8}copper-(I)) complex that contains short Cu(I)−Cu(I) separations of only2.539(2) Å.[47] There are numerous examples of Au(I)···Cu-(I) interactions in the literature, particularly in multimetallic cluster chemistry. In 1985 Abu-Salah et al.[48] reported the first Au(I)−Cu(I) alkynyl cluster containing heterometallic Au−Cu separations ranging from 2.783 to 3.016(3) Å. Yam and co-workers have thoroughly explored the photophysical properties of these and numerous related systems and noted similar separations.[49] Koshevoy and co-workers[50] have expanded this chemistry to produce a series of intensely luminescent, supramolecular Au−Cu "belts and rods" which contain both short Au−Au (2.86−2.87 Å) and multiple Au−Cu interactions (2.6867(7)−3.0421(7) Å). Likewise, Eisenberg and co-workers[11] reported short heterometallic distances of 2.634(1) and 2.646(1) Å in the pyridyl-coordinated Cu(I) and Au(I) center in [AuCu(μ-Spy)(μ-PPh$_2$py)]$^+$. Kappen et al.[51] reported the Cu(I) complex, [Pt(PPh$_3$)(AuPPh$_3$)$_6$(Cu$_4$I$_3$)]NO$_3$, that contains a multimetallic cluster with Au···Cu separations that range from 2.695 to 2.854 Å. Similar separations are found in CuAu-clusters. Copley and Mingos found Au−Cu separations ranging from 2.564(2) to 2.906(2) Å in the [Au$_9$Cu$_4$] cluster.[52] Coucouvanis and co-workers found longer Au(III)−Cu(I) separation in the [Cu$_4$Au] cluster ranging from 3.051(3) to 3.087(3) Å.[53]

As noted earlier, at room temperature the copper clusters dissociate from the gold complex upon dissolution

Scheme 4

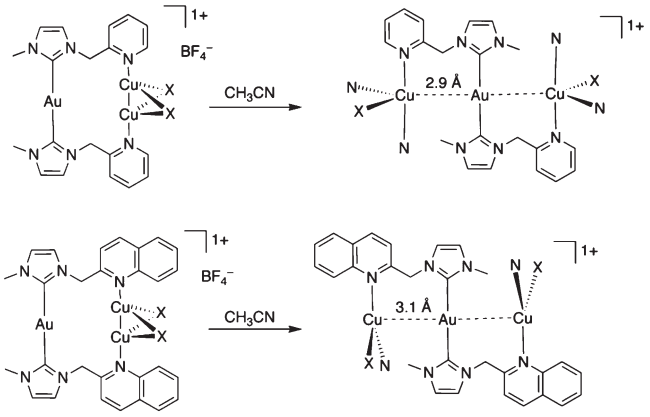

as demonstrated by the ^{1}H NMR spectroscopy. However, in frozen solution (20 K) the EXAFS and XANES data show that one Cu−X unit is coordinated to each imine donor along with one or two acetonitrile solvent molecules (Scheme 4). In each case the Au−Cu separations were ~3 Å, and no Cu−Cu interaction could be found. The ease at which the Cu−Cu linkage breaks is not surprising given the fluidity in which CuX moieties rearrange to form various cluster motifs.[26,54−57] The additional coordination of an acetonitrile to the picolyl complexes reflects the smaller steric encumbrance of this ligand relative to the quinolyl group. In fact, this observation is supported by the relative close separations of ~2.4 to 2.6 Å observed between the copper centers and the hydrogen atoms on the quinolyl 8-positions in complexes **3**− **5** (Figures 1-3).

The similar emission maxima of the Cu−X complexes make the assignment of the photoemissive state difficult. Changing the ligand from picolyl to quinolyl does not systematically red-shift the emission even though 2-methylquinoline is 600 mV easier to reduce[58] than 2-methylpyridine suggesting a purely MLCT state is unlikely. As noted by Araki et al.,[25] in their study of imine-Cu$_2$X$_2$ systems, the ligand redox potential does not always correlate to the excited state energy, particularly when the geometry around the metal changes. Likewise, because the emission does not follow the spectrochemical series for halide substitution, a purely halide-to-ligand charge transfer (XLCT) or a halide to metal charge transfer is equally unlikely. Excited states in copper clusters,[21−23] are known to originate from mixed orbital parentage, and there is no reason to exclude that possibility here. Further complicating the assignment are the observations that the ligand precursor and the copper-free materials are also photoluminescent in the solid-state. Finally, the inability to probe the emission of **4**−**6** or **9**−**11** in solution because of the dissociation of CuX makes it difficult to exclude the

(44) Healy, P. C.; Pakawatchai, C.; White, A. H. *J. Chem. Soc., Dalton Trans.* **1985**, 2531.
(45) Oshio, H.; Watanabe, T.; Ohto, A.; Ito, T.; Masuda, H. *Inorg. Chem.* **1996**, *35*, 462.
(46) Dyason, J. C.; Engelhardt, L. M.; Healy, P. C.; Pakawatchai, C.; White, A. H. *Inorg. Chem.* **1985**, *24*, 1950.
(47) Zhang, J.-F.; Yu, M.-M.; Chen, Y.; Ou, X.-M.; Fu, W.-F. *Acta Crystallogr., E: Struct. Rep. Online* **2006**, *62*, m2758.
(48) Abu-Salah, O. M.; Al-Ohaly, A.-R., A.; Knobler, C. B. *J. Organomet. Chem.* **1985**, 1502.
(49) Yip, S.-K.; Chan, C.-L.; Wai, H. L.; Cheung, K. K.; Yam, V. W.-W. *Photochem. Photobiol. Sci.* **2007**, *6*, 365.
(50) Koshevoy, I. O.; Koskinen, L.; Haukka, M.; Tunik, S. P.; Serdobintsev, P. Y.; Melnikov, A. S.; Pakkanen, T. A. *Angew. Chem., Int. Ed.* **2008**, *47*, 3942.
(51) Kappen, T. G. M. M.; Schlebos, P. P. J.; Bour, J. J.; Bosman, W. P.; Smits, J. M. M.; Beurskens, P. T.; Steggerda, J. J. *J. Am. Chem. Soc.* **1995**, *117*, 8327.
(52) Copley, R. C. B.; Mingos, D. M. P. *J. Chem. Soc., Dalton Trans.* **1996**, 479.
(53) Coucouvanis, D.; Kanodia, S.; Swenson, D.; Chen, S. J.; Stuedemann, T.; Baenziger, N. C.; Pedelty, R.; Chu, M. *J. Am. Chem. Soc.* **1993**, *115*, 11271.
(54) Kim, T. H.; Shin, Y. W.; Jung, J. H.; Kim, J. S.; Kim, J. *Angew. Chem., Int. Ed.* **2008**, *47*, 685.
(55) Kim, T. H.; Shin, Y. W.; Kim, J. S.; Lee, S. S.; Kim, J. *Inorg. Chem. Commun.* **2007**, *10*, 717.
(56) Lee, J. Y.; Lee, S. Y.; Sim, W.; Park, K.-M.; Kim, J.; Lee, S. S. *J. Am. Chem. Soc.* **2008**, *130*, 6902.
(57) Kim, T. H.; Shin, Y. W.; Lee, S. S.; Kim, J. *Inorg. Chem. Commun.* **2007**, *10*, 11.
(58) Tabner, B. J.; Yandle, J. R. *J. Chem. Soc. A* **1968**, 381.

role of intermolecular interactions. Clearly, more work in this area is needed before any reliable assignment can be made.

The results presented further support the utility of NHC ligands as supports for $d^{10}-d^{10}$ attractive interactions. We have shown that small, Cu_2X_2 butterfly clusters could be oriented in close proximity to a Au(I) center and that the resulting luminescence is significantly altered relative to the copper free materials, though the assignment of the excited remains elusive.

Acknowledgment. This work was supported by the National Science Foundation (CHE-0549902). Use of the National Synchrotron Light Source, BNL, was supported by the U.S. DOE, Office of Science, Office of Basic Energy Sciences under contract No. DE-AC02-98CH10886.

Supporting Information Available: X-ray crystallographic files in CIF format for **4**− **7** and **9**−**12** are available. This material is available free of charge via the Internet at http://pubs.acs.org.